Bull. Chem. Soc. Ethiop. **2025**, 39(5), 807-815.
DOI: https://dx.doi.org/10.4314/bcse.v39i5.1

ISSN 1011-3924
Printed in Ethiopia
Online ISSN 1726-801X

AN ENZYME-FREE ELECTROCHEMICAL GLUCOSE SENSOR BASED ON ORDERED POROUS Co_3O_4 MATERIAL

Jianzhi Sun[1,2,3*], Xinfang Wang[1,2,3], Dunqing Wang[1] and Min Yang[1]

[1]College of Chemistry and Chemical Engineering, Dezhou University, Shandong Dezhou, 253023, China
[2]Shandong Provincial Key Laboratory of Monocrystalline Silicon Semiconductor Materials and Technology, Dezhou, 253023, China
[3]Shandong Universities Engineering Research Center of Integrated Circuits Functional Materials and Expanded Applications, Dezhou, 253023, China

(Received July 1, 2024; Revised January 15, 2025; Accepted January 16, 2025)

ABSTRACT. In this paper, Co_3O_4 was synthesized through a one-step conversion from the precursor of Co-MOF, which was prepared using the liquid phase method. It was subsequently employed to construct a novel electrochemical sensor for glucose detection. The ordered pores in the material not only provided numerous electrocatalytic active sites but also facilitated the diffusion and desorption of electrolyte ions, glucose molecules, and intermediate products, thereby enhancing the overall electrocatalytic activity. Co_3O_4 demonstrated favorable electrocatalytic performance towards glucose oxidation. The fabricated sensor exhibited a sensitivity of 617.4 μA/(mmol·cm^2), with a detection limit as low as 0.23 μmol/L and a rapid response time within 5.9 seconds over a linear range from 0.62 μmol/L to 7.5 mmol/L. The sensor possesses several advantages including straightforward fabrication, satisfactory selectivity, and a low detection limit, thus broadening the application of metal-organic frameworks in the field of electrochemical sensing.

KEY WORDS: Ordered porous material, Co_3O_4, Electrochemical sensor, Non-enzymatic glucose sensors

INTRODUCTION

Glucose is the most widely distributed and important monosaccharide in nature, serves as the primary energy source for human and animal life processes. Blood glucose concentration is a critical indicator of human physiological health. Organisms can only carry out their normal functions if blood glucose levels are maintained within a certain range. Consequently, the precise monitoring of blood glucose levels is especially crucial for maintaining human health [1].

Diabetes has become one of the most common public health problems now days. Glucose concentration in human blood is one of the most key markers for the diagnoses and management of diabetes mellitus. Diagnosis of diabetes needs accurate and sensitive glucose detection. Currently, a myriad of techniques have been utilized to determine glucose, including chemiluminescence, fluorescence, high performance liquid chromatography (HPLC) and electrochemistry [2, 3]. Among these methods, the approach of electrochemical-based detection can allow a high sensitive in situ detection with short response time, wide linear range and low cost.

The enzyme sensors based on glucose oxidase have been widely used for the detection of glucose. The enzyme glucose sensor has the characteristics of high sensitivity and good selectivity [4, 5], but there are problems such as poor stability, complicated operation and poor repeatability. Therefore, non-enzymatic electrochemical glucose sensors have been gradually explored to improve the electrocatalytic activity towards the oxidation of glucose [6-10].

*Corresponding authors. E-mail: jianzhisun@163.com

The non-enzyme glucose sensor uses metal nanoparticles and their oxides as active substances instead of glucose oxidase to react with glucose [11]. However, most non-enzymatic sensors suffer from low sensitivity, high cost of rare metal precursors, poor specificity to glucose and so on. Among these non-enzymatic catalysts, transition metal oxides play important roles due to their high intrinsic catalytic performances, low cost, and environmental friendliness [12]. In the family of transition metal oxides, notably cobalt-based metal oxides are considered as promising candidates for the catalytic oxidation of glucose [13, 14].

The catalytic capability of the catalyst is not only associated with the intrinsic catalytic activity but it is also related to the morphology and structure. Recent studies showed that two-dimensional (2D) flake-like mesoporous structures exhibited many surpassing properties than that of other structures [15, 16]. The mesoporous structure with higher porosity and more available electroactive sites will provide more guest molecules (i.e., glucose) than other structures, enhancing the catalytic performances subsequently [17].

Co_3O_4 is a typical p-type transition metal oxide that contains both Co^{2+} and Co^{3+} ions. The mixed-valence structure endows it with sensitivity to electrocatalytic reactions [18-21]. In this paper, we first synthesized a two-dimensional sheet-structured metal-organic framework (Co-MOF) of cobalt, followed by the preparation of ordered porous Co_3O_4 sheets via calcination in air. A metal-organic framework (Co-MOF) of Co with a two-dimensional sheet structure was first synthesized, and then ordered porous Co_3O_4 sheets were prepared by calcination in the air. Subsequently, the as-prepared Co_3O_4 was applied to a glucose sensor, where its sensitivity, linear range, anti-interference capability, and other performance metrics were thoroughly investigated.

EXPERIMENTAL

Sample preparation

The materials used for the preparation of Co-MOF are cobalt(II) nitrate hexahydrate ($Co(NO_3)_2·6H_2O$) and N-methylimidazole ($C_4H_6N_2$). The precursor of Co-MOF was fabricated by a facile liquid phase process. In brief, turn the same volume of $Co(NO_3)_2$ solution (0.1 mol/L) into $C_4H_6N_2$ solution (0.1 mol/L) with agitation for 30 min and let it stand for about 10 hours at room temperature. Finally, the sample was calcined at 400 °C for 2 h at the heating rate of 0.5 °C/min in a muffle furnace, as shown in Figure 1.

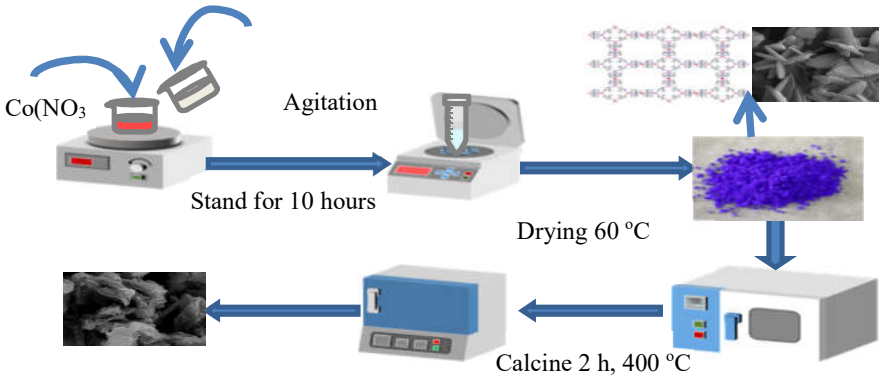

Figure 1. Preparation flow chart of the Co_3O_4 materials.

Preparation of Co_3O_4/GCE modified electrode

Prior to modification, the GCE electrode was polished with 0.05 μm α-Al_2O_3 powder to obtain a mirror-like surface, sonicated in ethanol and doubly distilled water, and then dried. Co_3O_4 was dispersed in Nafion solution (0.1%) and sonicated to form a homogenous mixture. Then 5 μL of 10 mg·mL^{-1} mixtures were dropped on the surface of GCE and air dry.

Characterization

X-Ray diffraction (XRD) was performed on a Bruker D8A25 X-Ray diffractometer. The X-ray beam was nickel-filtered Cu K (λ = 0.15406 nm) radiation operated at 40 kV and 30 mA; and the data were collected from 10 ° to 80 °(2θ) at a scanning rate of 5 °/min.

Thermal analysis (TG) was carried out on a NETZSCH STA 449 F5 equipment, operated under Air atmosphere. The samples were heated from room temperature up to 450 °C at heating rates of 10 °C/min.

The morphology of the samples was observed by JEOL JSM-5600LV SEM. EDX analysis was observed by Oxford Instruments.

Electrochemical sensor preparation and performance test

Electrochemical experiments were performed with a C16430 electrochemical workstation (Lvium Instruments, Netherlands). All experiments were conducted using a three-electrode electrochemical cell. Bare GCE or its modified electrode was used as the working electrode. A platinum plate electrode and an Ag/AgCl (3 mol/L KCl) electrode were used as counter and reference electrode, respectively. Prior to the electrochemical measurements, the solutions were deoxygenated by bubbling pure nitrogen gas for at least 20 min and a nitrogen atmosphere was kept over the solution during the experiments to eliminate the interference.

RESULTS AND DISCUSSION

Figure 2 shows the TG curves of the Co-MOF precursor heated from room temperature to 450 °C at a heating rate of 5 °C/min. Two-step mass losses are observed on the TG curve. The first mass loss is due to the evaporation of crystal water, which occurred at 30 °C to 295 °C. The second weight loss region occurs between 295 °C and 410 °C, which is due to the complete decomposition of the metal-organic framework (MOF) structure and its conversion into Co_3O_4. The chemical reaction that takes place involves the decomposition of the organic linker, releasing small molecule gases such as CO_2, H_2O, and nitrogen-containing compounds. Below is a simplified chemical equation to represent this process:

Co-MOF→ Co_3O_4 + CO_2 + H_2O + N-compounds

This transformation indicates that during thermal treatment within this temperature range, the organic components of the MOF decompose, leading to the formation of Cobalt tetraoxide along with the evolution of various gaseous by-products.

The X-ray diffraction (XRD) pattern of the Co-MOF precursor exhibited good agreement with reported data, confirming the successful synthesis of the precursor. Upon calcination, the color of the purple precursor changed to black, and this transformed sample was further characterized using XRD analysis. As shown in Figure 3, all diffraction peaks of 19°, 31.27°, 36.85°, 38.54°, 44.81°, 55.65°, 59.36°, 65.65°, 68.6°, and 69.73° can be indexed to the cubic phase of Co_3O_4, consistent with the standard card PDF No. 42-1467.

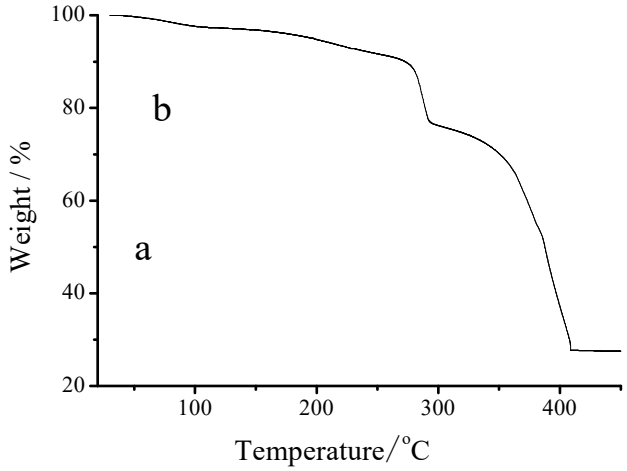

Figure 2. TG curves of the Co-MOF precursor.

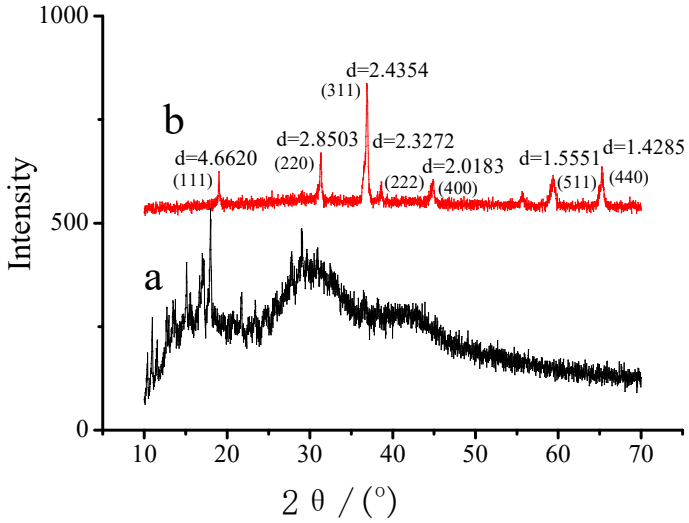

Figure 3. The XRD patterns of Co-MOF precursor and Co_3O_4 samples.

The morphological characteristics of the Co-MOF precursor and Co_3O_4 samples were investigated by SEM. As shown in Figure 4a, the Co-MOF exhibits a leaf-like structure, with individual flakes having a length of 5 to 6 μm and a width of approximately 2 μm. The Co_3O_4 samples not only present a two-dimensional sheet structure but also display a rich pore structure. It is clear that the flake is composed of porous structure inter-sectioned by Co_3O_4 nanocrystals at high magnification (Figure 4b). This structure effectively increases the specific surface area of the target product, thereby providing more catalytically active sites and enabling the efficient diffusion of electrolyte ions. In this pore structure, the transmission efficiency of electrocatalytic substances is greatly improved, thereby effectively improving the electrocatalytic activity of the Co_3O_4 porous material.

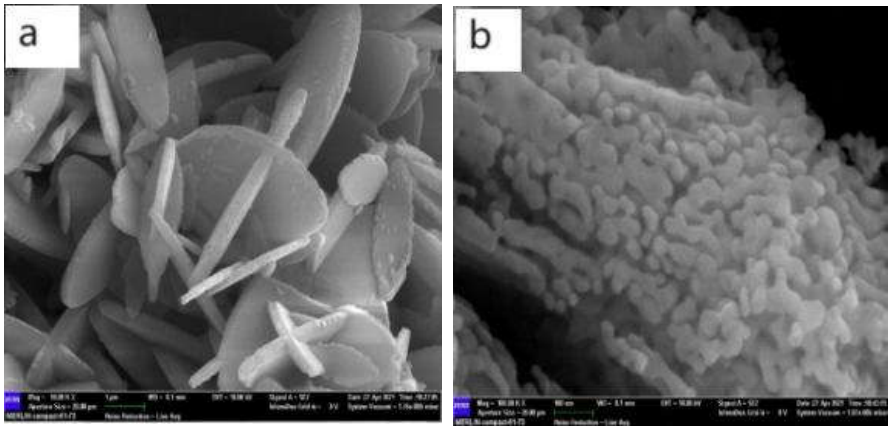

Figure 4. SEM images of Co-MOF precursor and Co_3O_4 samples.

Initially, the cyclic voltammetry (CV) was utilized in 0.1 mol/L NaOH electrolyte to investigate the electrochemical behaviors of the porous Co_3O_4/GCE under the applied potential from 0 to 0.6 V. As shown in Figure 5, a pair of apparent anodic peaks was observed at 0.42 V (curve 1), while the cathode peaks were at 0.54 V for porous Co_3O_4/GCE, which was ascribed to the reversible reactions of Co^{2+}/Co^{3+}. The curve 2 shows the electrochemical response of 0.5 mmol/L glucose on porous Co_3O_4/GCE at a scan rate of 20 mV/s. When the glucose was injected into the basic solution in Figure 5, the obvious electrochemical responses were detected (curve 2) compared to the blank solution (curve 1). Moreover, the curve 2 had a larger enclosed area than the curve 1, which indicated that the porous Co_3O_4/GCE had a higher chemical reactivity. The phenomenon demonstrates that porous Co_3O_4/GCE has the excellent catalytic capability to glucose.

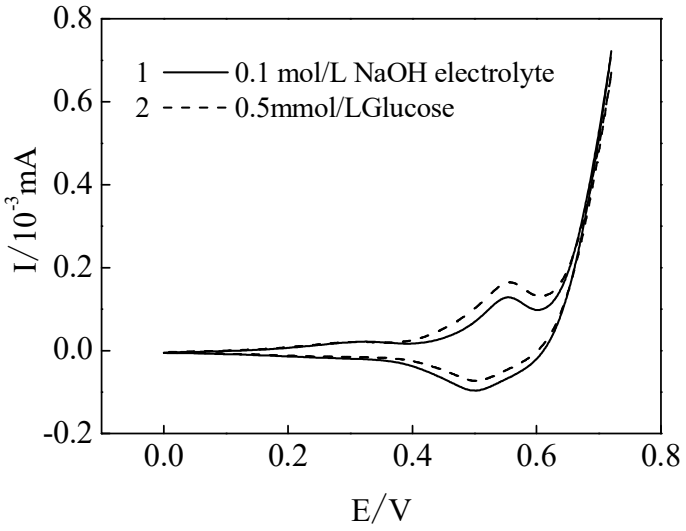

Figure 5. CV curves of porous Co_3O_4/GCE at a scan rate of 20 mV/s in 0.1 mol/L NaOH electrolyte.

In addition, peak 1 shifted to the right after the glucose was added. This phenomenon was caused by the adsorption of the intermediate product on the Co_3O_4/GCE surface and the limitation of the material transport kinetics. Based on the above analysis of the electrocatalytic mechanism, the size of the electrocatalytic current depends on the concentration of the medium CoO_2 that generates the electrons. Therefore, it can be inferred that the catalytic current reaches the maximum at the peak position of the oxidation peak. Therefore, the peak potential of the oxidation peak is 0.5 V.

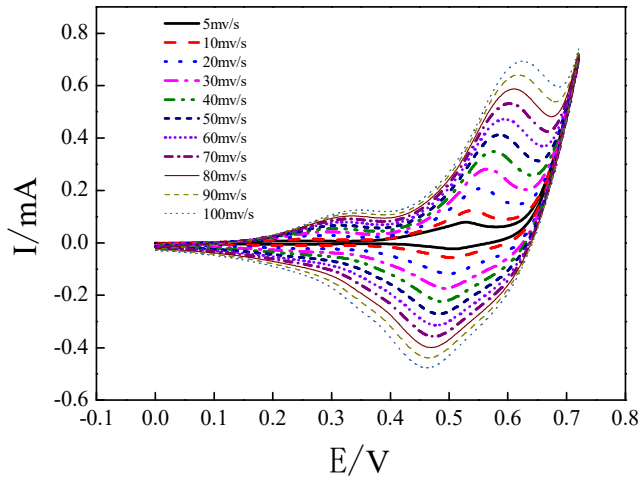

Figure 6. CV curves of Co_3O_4 with 5 mmol/L glucose at various scan rates.

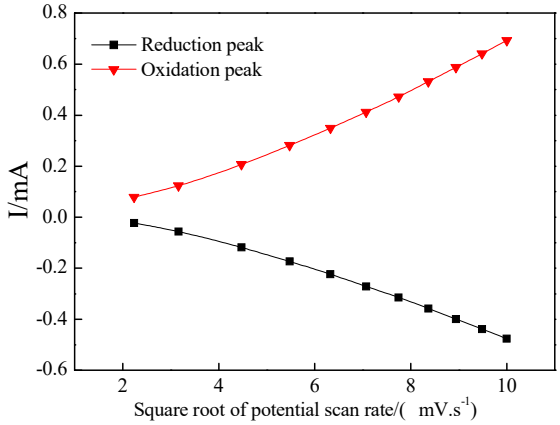

Figure 7. Corresponding plots of anodic peak currents versus square root of potential scan rate in the presence of 5 mmol/L glucose.

In order to further confirm the electrocatalytic kinetic control process of the electrode, the kinetic analysis of the as-prepared electrodes was investigated by CV and chronoamperometry response in 0.1 mol/L NaOH solution, as shown in Figure 6. The relationship between the peak current and the square root of the scanning speed is shown in Figure 7. It can be seen from the figure that the peak currents of peaks are proportional to the square root of the scanning speed,

which shows that the electrode surface is a typical diffusion control process. In addition, as the scanning speed increases, the peak potential of the oxidation peak shifts to the right, and the peak potential of the reduction peak shifts to the left, indicating that the electrochemical process has a dynamic relaxation phenomenon, which is a quasi-reversible process.

Figure 8 is to determine the sensitivity and linear range of Co_3O_4/GCE for glucose detection. Different concentrations of glucose solutions are continuously dripped into a 0.1 mol/L NaOH solution by chronoamperometry. It can be seen from the figure that when glucose is added to the solution, the current signal increases rapidly, indicating that the electrode has a higher electrocatalytic activity for glucose.

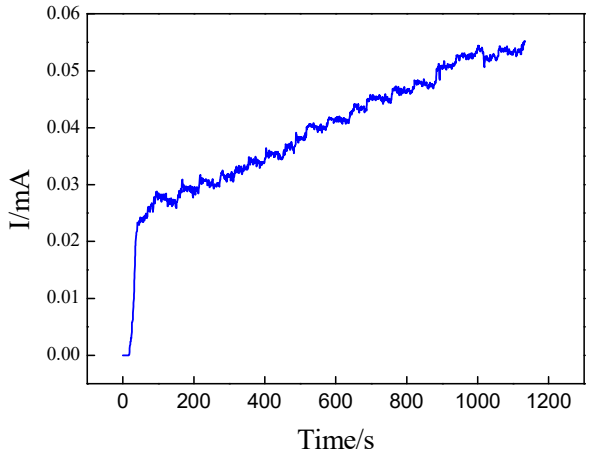

Figure 8. Chronoamperometric current responses of Co_3O_4/GCE to successive injection of various concentrations of glucose into 0.1 mol /L NaOH at 0.56 V under a constant stirring rate.

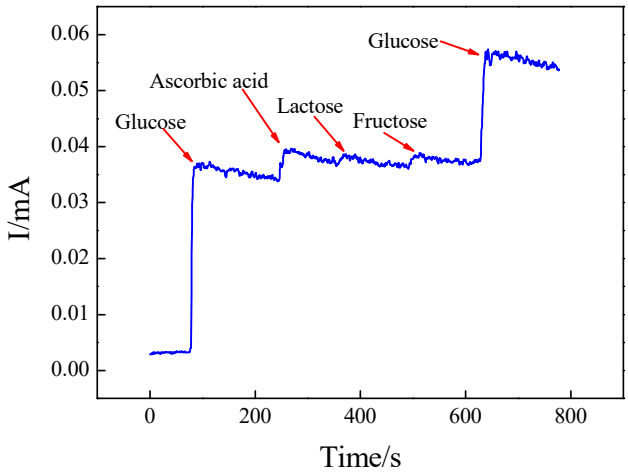

Figure 9. Anti-jamming test results of sheet Co_3O_4/GCE.

Compared to enzyme-based glucose sensors, which exhibit good selectivity, non-enzymatic glucose sensors encounter significant challenges in environments containing coexisting substances. Human blood contains numerous trace interfering compounds, making the investigation of anti-interference properties for Co_3O_4/GCE critically important. As illustrated in Figure 9, when 1 mmol/L glucose is introduced into a 0.1 mol/L NaOH solution, followed by additions of 0.1 mmol/L ascorbic acid, 0.1 mmol/L lactose, and 0.1 mmol/L fructose, the figure demonstrates that the response currents from these potential interfering substances are minimal and almost negligible compared to that of glucose. Consequently, this indicates that Co_3O_4/GCE exhibits excellent anti-interference performance.

CONCLUSION

In summary, a Co-MOF precursor combined with a facile heat treatment method was successfully developed to construct a Co_3O_4 non-enzymatic glucose sensor. This material possesses a two-dimensional sheet structure along with numerous microscopic pores. The glucose sensor fabricated using this approach demonstrates exceptional stability and selectivity. The enhancement in electrode performance can be attributed to its distinctive two-dimensional architecture and porous nature. Specifically, the two-dimensional structural features facilitate efficient electron transfer and collection, whereas the porous structure enhances material transport kinetics. The controlled microstructure significantly influences the electrocatalytic activity; by optimizing these characteristics, we can boost the electrocatalytic performance. Therefore, the ordered porous Co_3O_4 electrode represents a promising candidate for practical application in non-enzymatic glucose sensing.

ACKNOWLEDGEMENTS

The authors acknowledge financial assistance from the Undergraduate University Teaching Reform Research Project of Shandong (Z2023188) and the Natural Science Foundation of Shandong (ZR2020MB134).

REFERENCES

1. Liang, Z.; Zhang, J.Y.; Wu, C. Flexible and self-healing electrochemical hydrogel sensor with high efficiency toward glucose monitoring. *Biosens. Bioelectron*. **2020**, 155, 112105.
2. Mousavizadegan, M.; Asiabi, P.A.; Hosseini, M. Synthesis of magnetic silk nanostructures with peroxidase like activity as an approach for the detection of glucose. *Chemistry Select* **2020**, 5, 8093-8098.
3. Namli, S.; Sumnu, S.G.; Oztop, M.H. Microwave glycation of soy protein isolate with rare sugar (D-allulose) fructose and glucose. *Food Biosci*. **2021**, 40, 100897-100899.
4. Lee, J.H.; Oh, B.K.; Choi, B. Electrical detection-based analytic biodevice technology. *BioChip J*. **2010**, 4, 1-8.
5. Li, X.D.; Pang, J.W. Preparation of flower-like hierarchical structure SnO_2/g-C_3N_4 and its ethanol gas-sensitive properties. *Bull. Chem. Soc. Ethiop*. **2025**, 39, 141-152.
6. Vilian, A.T.E.; Hwang, S.K.; Ranjith, K.S. A facile method for the fabrication of hierarchically structured Ni_2CoS_4 nanopetals on carbon nanofibers to enhance non-enzymatic glucose oxidation. *Mikrochim. Acta* **2021**, 188, 10601-10610.
7. Bekele, G.; Tsegaye, A.A.; Taddesse, A.M.; Teju, E. A stable electrochemical sensor for the detection of ascorbic acid based on Fe_3O_4/ZrO_2 nano composite modified carbon paste electrode. *Bull. Chem. Soc. Ethiop*. **2024**, 38, 1205-1223.
8. Dayaker, T.; Rao, K.V.; Bishalu, K. Non-enzymatic sensing of glucose using screen-printed electrode modified with novel synthesized CeO_2@CuO core shell nanostructure. *Biosens. Bioelectron.* **2018**, 111, 166-173.

9. Mahbob, E.N.M.; Ahmad, M.S.; Isa, I.M.; Hashim, N.; Ul-Hamid, A.; Saidin, M.I.; Si, S. M. Electrochemical sensor of multiwalled carbon nanotube electrode modified by 1-phenyl-3-methyl-4-orthofluoro benzoyl-5-pyrazolone for sensing dopamine. *Bull. Chem. Soc. Ethiop*. **2023**, 37, 845-857.
10. Sun, Y.; Zhang, Y.; Ren, H.; Qiu, H.; Zhang, S.; Lu, Q.; Hu, Y. Highly sensitive SERS sensors for glucose detection based on enzyme@MOFs and ratiometric Raman. *Talanta* **2024**, 271, 125647.
11. Yin, H.Y.; Zhan, T.Y.; Chen, J.L. Polyhedral NiO/C porous composites derived by controlled pyrolysis of Ni-MOF for highly efficient non-enzymatic glucose detection. *J. Mater. Sci. Mater. Electron.* **2020**, 31, 4323-4335.
12. Wang, H.; Qiu, J.; Sun, S. A non-enzymatic glucose sensor based on Ni/PANI coaxial nanowire arrays. *J. Mater. Sci. Mater. Electron.* **2021**, 32, 7751-7764.
13. Husain, A.Z.; Al-Jawaheri, Y.S.; Al-Assafe, A.Y. Synthesis of substituted 2-amino oxazoles with their cobalt(II) and platinum(IV) complexes and evaluation of their biological activity. *Bull. Chem. Soc. Ethiop.* **2024**, 38, 1667-1680.
14. Nimal, R.J.G.R.; Jose, D.F.M.; Balasubramanian, K.; Sunil, J. Evaluation of improved corrosion resistance of Zn alloy as electrode material by Co_3O_4 coatings. *Bull. Chem. Soc. Ethiop*. **2024**, 38, 241-253.
15. Naik, K.K.; Kumar, S.; Rout, C.S.; Electrodeposited spinel $NiCo_2O_4$ nanosheet arrays for glucose sensing application. *RSC Adv*. **2015**, 5, 74585-74591.
16. Prathap, M.U.A.; Wei, C.; Sun, S. A new insight into electrochemical detection of eugenol by hierarchical sheaf-like mesoporous $NiCo_2O_4$. *Nano Res*. **2015**, 8, 2636-2645.
17. Deng, W.; Yuan, X.; Tan, Y. Three-dimensional graphene-like carbon frameworks as a new electrode material for electrochemical determination of small biomolecules. *Biosens. Bioelectron*. **2016**, 85, 618-624.
18. Umar, A.; Rauts, D.; Ibrahim, A.A. Perforated Co_3O_4 nanosheets as high-performing supercapacitor material. *Electrochim. Acta* **2021**, 389, 138661.
19. Zheng, S.S.; Li, X.R.; Yan, B.Y. Transition-metal (Fe,Co,Ni) based metal-organic frameworks for electrochemical energy storage. *Adv. Energy Mater*. **2017,** 18, 1602733.
20. Geng, C.; Wei, P.; Chen, H.M. Promoting the hole extraction and interfacial performance with MOFs derived Co_3O_4@NC for efficient carbon-based perovskite solar cells. *Chem. Eng. J.* **2021**, 414, 128878.
21. Luo, S.J.; Li, X.M.; Zhang, B.H. MOF-derived Co_3O_4@NC with core-shells tructures for N_2 electrochemical reduction under ambient conditions. *ACS Appl. Mater. Interfaces* **2019**, 11, 26891-26897.